Journal of Power Sources 239 (2013) 696–704

Contents lists available at SciVerse ScienceDirect

Journal of Power Sources

journal homepage: www.elsevier.com/locate/jpowsour

Analysis and prediction of the open circuit potential of lithium-ion cells

Jan Philipp Schmidt [a,*], Hai Yen Tran [b], Jan Richter [a], Ellen Ivers-Tiffée [a], Margret Wohlfahrt-Mehrens [b]

[a] Institut für Werkstoffe der Elektrotechnik (IWE), Karlsruhe Institute of Technology (KIT), D-76131 Karlsruhe, Germany
[b] ZSW-Center for Solar Energy and Hydrogen Research, Helmholtzstrasse 8, D-89081 Ulm, Germany

HIGHLIGHTS

- A model for the quantitative OCV analysis of Li-ion cells is introduced.
- In-situ diagnosis of aging mechanisms is experimentally verified.
- Loss of active lithium and contact loss of active material are separated.
- A novel model to describe the OCV of a blend cathode is introduced.
- The active masses of the blend components are determined using the OCV model.

ARTICLE INFO

Article history:
Received 18 September 2012
Received in revised form
9 November 2012
Accepted 23 November 2012
Available online 29 November 2012

Keywords:
Lithium-ion
Open circuit potential
Model
Diagnosis
Blend
Analysis

ABSTRACT

A model is presented, which allows quantitative analysis as well as prediction of the open circuit potential of lithium-ion cells. Furthermore, the model determines half-cell potentials of already stressed lithium-ion cells, using a data set accomplished just once from half-cell potentials of a new reference cell. Its capability to describe thereby two relevant degradation processes, namely, (i) loss of active mass, and, (ii) loss of active lithium, is experimentally verified on a $LiNi_{0.8}Co_{0.15}Al_{0.05}O_2$ (NCA)/$LiCoO_2$ (LCO) blend cell.

A further extension of the model allows the prediction of the open circuit potential of a blend cathode with various blend ratios as well as the analysis of unknown blend ratios. This ability is experimentally verified for cathodes made of $LiNi_{0.8}Co_{0.15}Al_{0.05}O_2$ (NCA)/$LiMn_2O_4$ (LMO) blends.

1. Introduction

Two relevant degradation processes, namely, (i) loss of active mass, and, (ii) loss of active lithium, affect the open circuit potential (OCV) of lithium-ion cells. In experimental cells, these changes are usually monitored by a standard reference electrode [1], using a piece of metallic lithium attached to a copper wire [2,3], electrochemically deposited lithium [4] or lithium-metal alloy [5,6]. However, the reference electrode itself is a source of error, since the reference material may interfere with the chemical and electrical electrode characteristics. However, reference electrodes are widely used to extract the half-cell potentials of anode and cathode in experimental cells, but their applicability in commercial cells is of questionable value.

In this case, the commercial cell (i) has to be opened, (ii) the reference electrode has to be inserted in the electrode stack or role, (iii) lost electrolyte has to be refilled, and finally, (iv) the cell has to be sealed again [7]. This rather complicated process influences the cell behavior, as the content of active lithium may be changed, and thus, the half-cell potentials of the electrodes deviate from the original course.

To overcome those obstacles, we apply a model based on [8], which enables online analysis of the half-cell potential of commercial cells during cycling with small currents. The model requires a data set containing the half-cell potentials of the relevant anode and cathode materials, which has to be determined over SOC by a separate measurement. Therefore, and just once, a commercial cell has to be opened, and both electrodes are measured in experimental half-cells. This data set is then available for calculating the change of half-cell potentials of new cells during their entire lifetime. Thus, a real-time analysis of degradation mechanisms

* Corresponding author. Tel.: +49 721 608 47583; fax: +49 721 608 47492.
E-mail address: jan.schmidt@kit.edu (J.P. Schmidt).

0378-7753/$ – see front matter © 2012 Elsevier B.V. All rights reserved.
http://dx.doi.org/10.1016/j.jpowsour.2012.11.101

becomes possible, as a recent publication of Dubarry et al. [9] has already shown by simulation. Herein, loss mechanisms became identifiable from OCV-curve measurements, on condition that the half-cell potentials are known. For the first time, our findings proof the applicability to real measurements.

In case of a lithium-ion cell with a cathode blend, which usually consists of two active materials [10,11], the mixed open circuit potential depends on blend ratio and material chemistry. Thereby, tailoring of open circuit potentials becomes possible. It is evident, that a model which predicts the open circuit potential of arbitrary blends is beneficial to determine the blend ratio prior to manufacturing.

Likewise such a model can be potentially applied to determine the composition and blend ratio of unknown cathodes. Furthermore, such a model can identify the degradation of single blend components using differential capacity plots [12].

In the following, we introduce first the so-called *OCV-model full cell* for analysis and prediction of the open circuit potential a full cell. Second, we introduce a sub-model called *OCV-model blend electrode*, which is tested on cathode blends. Its outcome is an OCV-curve, where the half-cell potential of the blend electrode is measured versus lithium, which is then integrated into the *OCV-model full cell*.

2. OCV-model full cell

2.1. Theory

The potential of a full cell $U_{\text{full}}(Q)$ in dependence of the charged capacity Q is expressed as the potentials of the half-cells:

$$U_{\text{full}}(Q) = U_{\text{cat}}(Q) - U_{\text{an}}(Q). \quad (1)$$

If the potential $U_{\text{cat}}(Q)$ and $U_{\text{an}}(Q)$ vs. lithium of the half-cells is measured as function of the charged capacity, the full cell potential can then be calculated [8,13,14] using Equation (1). For different capacities of anode $Q_{0,\text{an}}$ and cathode $Q_{0,\text{cat}}$, the smaller electrode or the available amount of lithium-ions determines the full cell capacity. Thereby, the OCV curve of the full cell is calculated by using a set of measured OCV curves of anode and cathode.

However, if the capacity of one electrode is altered, the actual OCV curve of the corresponding half-cell must be measured. To avoid any new measurement over time, it is much advantageous to multiply the charged capacity Q by a scaling factor α_{cat} and α_{an} in Equation (2). This multiplication results in a scaling of the OCV curve with the Q-axis, as it is shown in Fig. 1. The capacity ratio of the simulated full cell can then be easily calculated as

$$c_{\text{an/cat}} = \frac{Q_{0,\text{an}} \cdot \alpha_{\text{an}}}{Q_{0,\text{cat}} \cdot \alpha_{\text{cat}}}. \quad (2)$$

Furthermore, as the cathode is not necessarily completely discharged, when the anode is charged and the full cell state is completely charged. This is sometimes called “alignment” of the electrodes. To account for that, the two parameters ν_{cat} and ν_{an} are introduced. Equation (3) describes now the complete model for the potential of a full cell $U_{\text{full}}(Q)$, and the resulting OCV curve is illustrated in Fig. 1.

$$U_{\text{full}}(Q) = U_{\text{cat}}(\alpha_{\text{cat}}Q - \nu_{\text{cat}}) - U_{\text{an}}(\alpha_{\text{an}}Q - \nu_{\text{an}}) \quad (3)$$

The model Equation (3) is now applicable for the simulation of full cell potentials for electrode combinations of any chemistry. Furthermore, if the OCV curves of the chosen anode and cathode material are available from separate measurements, these data sets can be used to identify the model parameters α_{cat}, α_{an}, ν_{cat} and ν_{an}. These parameters are obtained by fitting the resulting full cell potential from Equation (3) and the underlying anode and cathode OCV-curves to the measured full cell potential. With those parameters the half-cell potential for every charged capacity can now be evaluated by separately evaluating the terms for U_{cat} and U_{an}.

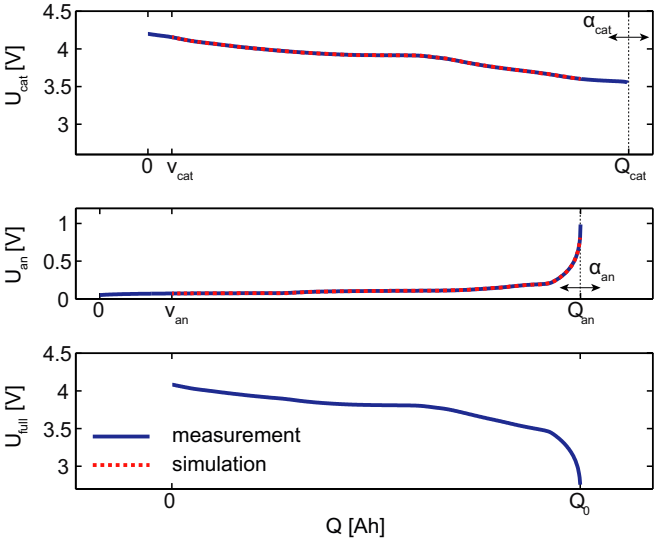

Fig. 1. Schematic of the OCV model full cell, which is calculated from two separate OCV curves of cathode and anode. The parameters α_{cat} and α_{an} are used to scale the capacity and ν_{cat} and ν_{an} to adjust the alignment of the single electrodes. The resulting full cell OCV curve is computed by subtracting the cathode from the anode potential.

Since Equation (3) is only valid at equilibrium, all OCV-curves, from half- and full-cells, have to be obtained with low discharge or charge rates, ensuring close-to equilibrium conditions. At higher currents the characteristic steps in the OCV-curves are flattened, which complicates the identification of the model parameters. Furthermore, overpotentials arising from solid-state diffusion and charge transfer are superimposed to the open circuit voltage. The effect on the fitting result can be alleviated to some extent by choosing identical C-rates for the measurement of the OCV-curves of the half-cells and the full cell.

2.2. Experimental

All electrodes were obtained from Kokam SLPB834374H lithium-ion cells with a capacity of 2 Ah. They were disassembled in an Argon filled Glovebox (Braun, Germany) and experimental cells with a diameter of 18 mm were built immediately. The cell housings ECC-Ref (el-cell, Germany) were equipped with a lithium reference electrode. As separator three Freudenberg FS2190 were used and 250 μl of LP50 (Merck, Germany) was used as electrolyte. The liquid electrolyte was composed of a 1 mol l^{-1} LiPF6-solution in a 1:1 mixing ratio with ethylene carbonate:ethylmethyl carbonate (EC:EMC).

At first, two experimental cells were built with anode and cathode material from the commercial cell versus a lithium counter electrode. Then half-cell potentials during constant current charge and discharge with a C-rate of C/40 were recorded.

These two measurements are of great importance, as they serve as reference OCV curves of anode and cathode for the once required parameterization of the *OCV model full-cell*.

The next step, the validation of the *OCV model full-cell*, required two further experiments, namely, a variation in (a) the active mass of lithium and (b) the active mass of the cathode. The variation in (a) the active mass of lithium represents cell aging correlated to

side reactions, as reported in Refs. [15–17]. The variation in (b) the active mass of the cathode simulates cell aging correlated to a decreasing contact area between or inside cathode particles [18]. These two experiments, which are appropriate to demonstrate the practicability of the *OCV model full-cell* in actual fields of research, are described in detail in the following.

(a) Variation of active mass of lithium

The variation of the active mass of lithium required disassembling three commercial cells, which were preset to SOC of 0%, 80% and, 60%, respectively:

- Cell 1 was discharged at 1 C to the discharge stop criterion of 2.7 V, resulting in a state of charge of the full cell of SOC = 0% and an active lithium-ion content in the cathode of 100%.
- Cell 2 was discharged at 1 C until 80% of the capacity of cell 1 was withdrawn, resulting in SOC = 20% and an active lithium-ion content in the cathode of 80%.
- Cell 3 was discharged at 1 C until 60% of the capacity of cell 1 was withdrawn, resulting in SOC = 40% and an active lithium-ion content in the cathode of 60%.

Of the cathode of those three disassembled cells, three experimental cells were built with an anode from cell 1, resulting in a variation of the active lithium-ion content in those experimental cell from 100% to 60%. For all three experimental cells charge and discharge curves with a constant current I_{const} of 99 μA were measured using a Solartron 1470E cell test system (Solartron Analytical, UK) and the potential of the lithium reference electrode vs. the cathode and anode was recorded.

(b) Variation of the active mass of the cathode

For this variation, only the disassembled cathode layer from commercial cell 1, which was discharged to SOC = 0%, was used. In the first step, three cathodes with a diameter of 18 mm were punched out. In the second step, the active mass of these cathodes was reduced by punching out a varying number of small circles with a diameter of 5 mm each, as depicted in Fig. 2. Thereby, the active mass of cathode was reduced to 92%, 85%, and, 77% compared to the original cathode. Naturally, we adapted the C-rates to the respective changes of the active surface area, which is proportional to the change in active mass of the cathode. Thereby, a comparable overpotential among all experiments was achieved, and the resulting C-rates and currents I_{const} are reported in Table 1. While for the cell with an active surface area of 2.35 cm^2 (92% active mass) the same C-rate was achieved, for the cells with an active surface of 2.15 cm^2 (85%) and 1.96 cm^2 (77%) the C-rate was slightly higher but still close to the original C/40-rate and compensates for most of the loss of active area.

Table 1 gives an overview over all experiments made with a variation in (a) active mass of lithium and (b) of cathode, respectively, referencing the figures where the results are displayed.

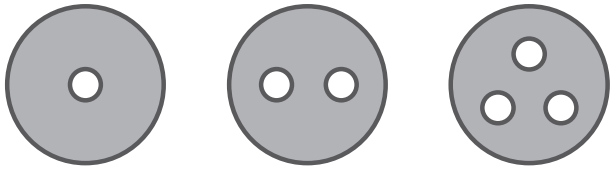

Fig. 2. Schematic showing the variation of the active mass of the cathode. This is realized by punching 1, 2, or 3 holes (d = 5 mm) into the cathode (d = 18 mm), and results into an active mass of 92%, 85%, and, 77% compared to the original cathode with 100% active mass.

Table 1
Experimental cells built from cathodes and anodes harvested from three commercial 18,650 cells, including a variation in the active mass of lithium and of cathode material. I_{const}: constant charging current, C-rate: relation of constant charging current to actual capacity, Q: measured capacity for a full charge.

Active mass cathode [%]	Active mass lithium [%]	I_{const} [μA]	Q [C]	C-rate	Figure
100	100	99	13.04	C/37	3
100	80	99	10.92	C/31	Not displayed
100	60	99	7.83	C/22	3
92	100	91	13.27	C/40	Not displayed
85	100	83	11.01	C/37	4
77	100	76	9.99	C/37	4

2.3. Results

In the following, we present first the parameterization step for the OCV model full cell, followed by the extraction of the model parameters α_{cat}, α_{an}, ν_{cat} and ν_{an}.

Fig. 3 shows measurements of and simulations for experimental cells with an active mass of lithium of 100% (left) and 60% (right). The measured full cell potential, and both half-cell potentials for cathode and anode, which are important for the parameterization of the OCV model full-cell, are depicted as a blue line (in the web version). As supposed, the experimental cell with the active mass of lithium of 60% has a reduced full cell capacity, when compared to the experimental cell with an active mass of lithium of 100%. Both OCV curves constitute the basis for the following fitting procedure with Equation (3), whereby the parameterization is performed based on the reference half-cell potentials of anode and cathode, and using a proprietary algorithm implemented in Matlab (MathWorks, USA). The obtained model parameters α_{cat}, α_{an}, ν_{cat} and ν_{an} are now used to calculate the half-cell potentials of both electrodes as well as the full cell potential, these results are depicted as a red line (in the web version) in Fig. 3. Deviations between measured and simulated potentials stay always below 0.5%, indicating a very good fit quality.

Furthermore, all six diagrams in Fig. 3 show a window indicated by dotted black lines which varies with the active mass of lithium. However, the capacity of the simulated half-cell potentials for anode and cathode remains about the same for both experimental cells. In other words, the *OCV model full-cell* describes reality, as the variation of the active mass of lithium has no effect on the capacity of the active mass of anode and cathode. Therefore, the correctness of the *OCV model full-cell* is confirmed by (i) the good fit quality of both half-cell potential and full-cell potential and by (ii) the representation of the fading mechanism of active mass of lithium. As the simulation results show that the active mass of anode and cathode remains unchanged, it is concluded that the model is capable to identify the loss of active lithium.

Fig. 4 shows now the results of measured (blue line in the web version) and simulated OCV curves (red line in the web version) for two variations of the active mass of the cathode (92% and 85%). For 92% (left), the OCV curves for full cell and both half-cells coincide excellent over the entire charging range. This holds true for the full cell potential at an active mass of the cathode of 85% as well. However, signal noise is visible for both measured half-cell potentials at charges <0.5 mAh. It is noteworthy, that both simulated half-cell potentials are free of noise, since they are calculated from the full-cell potential. Therefore, the signal noise is considered as measurement error, originating from an inferior contact of the lithium reference electrode. Interesting enough, in this case, the

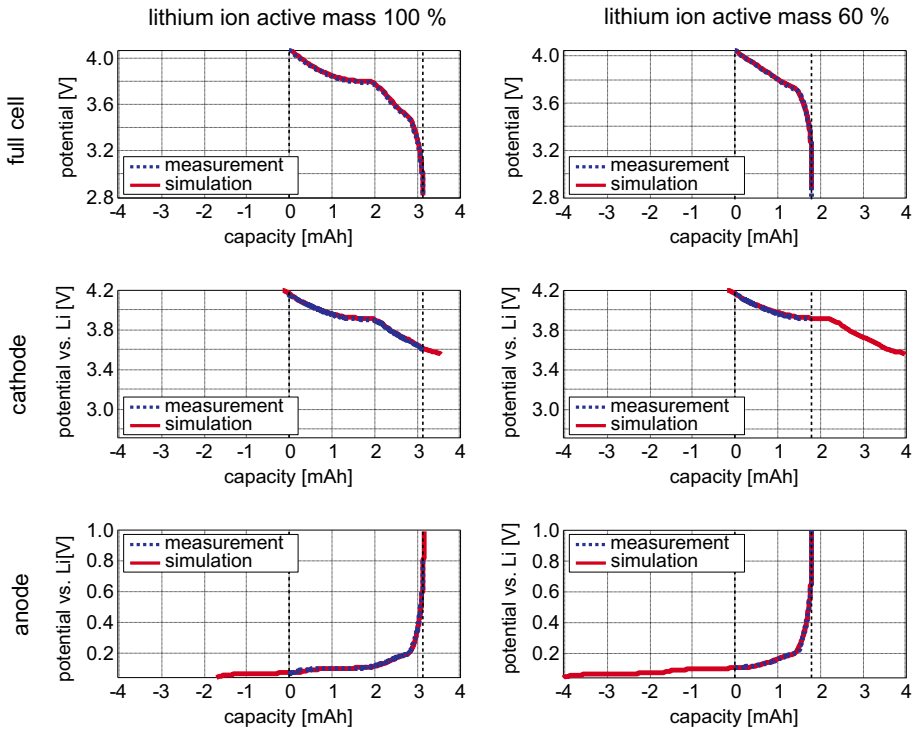

Fig. 3. Measured and simulated potentials for a variation of active lithium-ion content. The red lines depict the simulated potentials and the dotted blue lines the measured potentials. (For interpretation of the references to color in this figure legend, the reader is referred to the web version of this article.)

simulated OCV curve delivers more accurate values than the measured one. As in Fig. 3, all six diagrams in Fig. 4 show a window indicated by dotted black lines. In this experiment, the utilized active lithium-ion content (charge between the black dotted lines) as well as the capacity of the active mass of the cathode varies. It can be concluded, that the *OCV model full-cell* describes the loss of active material in the cathode correctly and allows distinguishing between both types of material cutbacks.

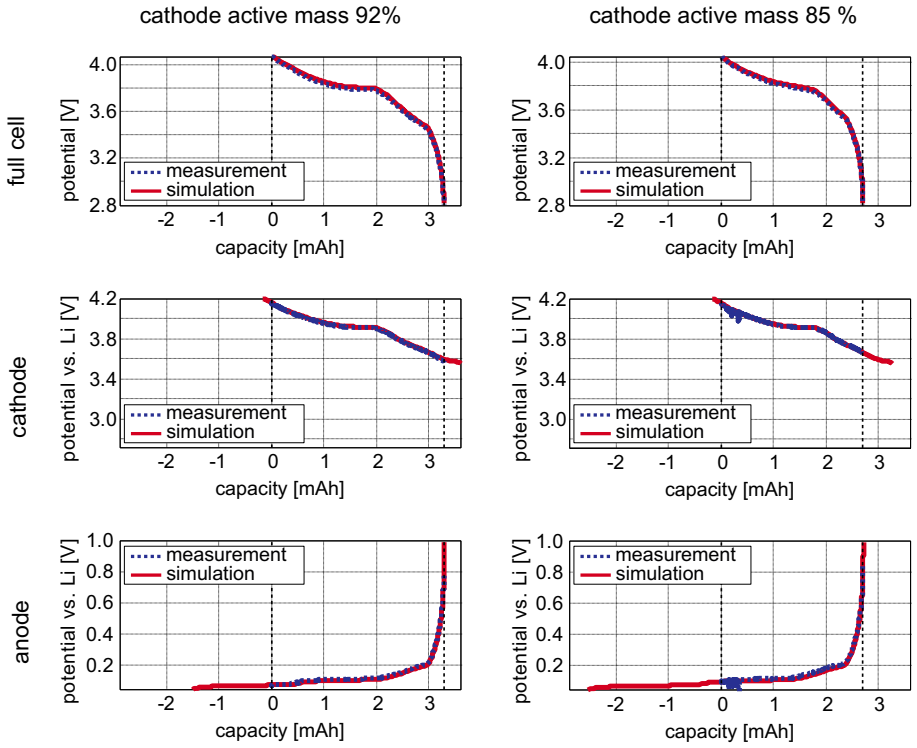

Fig. 4. Measured and simulated potentials for a variation of the active mass of the cathode. The red lines depict the simulated potentials and the dotted blue lines the measured potentials. (For interpretation of the references to color in this figure legend, the reader is referred to the web version of this article.)

As both loss of active lithium and contact loss of active material decrease the available full cell capacity, identification of degradation mechanism requires additional information. This additional information is obtained via the *OCV model full-cell*, with the capacities of anode and cathode. Fig. 5a) displays the measured full cell capacities of the variation of the active lithium content and Fig. 5b) of the variation of the cathode active mass. For both cases the full cell capacity decreases with increasing impact of the simulated degradation mechanism. For the variation of cathode active mass, the cathode capacity decreases with the same rate as the full cell capacity. However for the variation of the active lithium content the cathode capacity even increases slightly. As the cathode active mass has not been changed by the experimental setup, this increase is regarded as an influence of the preparation. Nevertheless a distinction of both degradation mechanisms from the correlation of full cell capacity and cathode capacity could be achieved. This demonstrates applicability of the model for the investigation of cell degradation in large scale field tests, without the need of a lithium reference electrode. This model is applicable for a variety of cathode chemistries and blends thereof, as it is based on measured OCV curves only. In general, the sensitivity of the model depends on the dissimilarity of the half-cell OCVs. We conclude from the case studies in Ref. [9], that this model should be also applicable to LiFePO4-cathodes. Furthermore, the aging of blend electrodes becomes accessible by an extension of this rather simple model, as shown next.

3. OCV-model blend electrode

3.1. Theory

To understand how the OCV curve of a blend electrode is gained from the OCVs of its two constituents, it is advantageous to follow the course of the differential intercalation capacity $C_{\Delta Int}$. It is obtained in Equation (4) by differentiating the open circuit potential U with respect to the accumulated charge Q [19] and forming the reciprocal:

$$C_{\Delta Int}(U) = \frac{dQ}{dU}. \tag{4}$$

Fig. 6 depicts the OCV curve of a graphite anode versus the accumulated charge Q (left) the corresponding differential intercalation capacity $C_{\Delta Int}$ plot (right); the anode was discharged at a low C-rate of C/40. Plateaus in the open circuit potential are well reflected by peaks in the differential intercalation capacity. It is concluded, that the area beneath a peak represents the charge which is stored in a certain stage. For the sake of clarity, we have plotted the potential versus $C_{\Delta Int}$, whereas normally $C_{\Delta Int}$ is plotted over the potential.

Using the differential intercalation capacity $C_{\Delta Int}$ the *OCV model blend cathode* is now derived by setting up an equivalent circuit model (ECM). In general, transport processes like charge transfer of ions and electrons across interfaces, ionic transport in the electrolyte or solid state diffusion processes in anode or cathode are described herein by specific circuit elements. The simplest ECM for a lithium-ion cell, depicted in Fig. 7a, consists of a complex impedance Z_{cell}, which summarizes all individual dynamic processes, and a potential source as representation of the OCV where the OCV is mapped as function of the accumulated charge. As demonstrated before, this can be transformed to the differential intercalation capacity and the potential source is replaced with a capacitance (compare Fig. 7b). Hereby, the cell voltage changes with the accumulated charge, which is calculated by integrating the cell current. Last but not least, for simulating the OCV curve of a cathode blend, two controlled capacities and two complex impedances, Z_1 and Z_2, are introduced. Now it is possible, to describe a blend electrode with two different active materials as parallel connection of two equivalent circuits from Fig. 7b resulting in the circuit presented in Fig. 7c.

It has to be noted, that the following approach is only valid if the current passing through the cell is assumed to be negligible small and hence Z_1 and Z_2 are negligible small, too. As we intend to model the OCV, which is defined as potential under equilibrium conditions, this precondition is fulfilled.

By neglecting the complex impedance Z_1 and Z_2, the resulting capacity $C_{\Delta Int,blend}$ is obtained by substitution of the individual capacities $C_{\Delta Int,1}$, $C_{\Delta Int,2}$ and it can be calculated as

$$C_{\Delta Int,blend}(U) = \beta_1 C_{\Delta Int,1}(U) + \beta_2 C_{\Delta Int,2}(U). \tag{5}$$

Herein the coefficients β_i are used to scale the mass of the individual blend components.

The OCV curve $U_{OCV,blend}$ is calculated by using the integral Equation (6)

$$Q_{OCV,blend}(U) = \int_{U_{min}}^{U_{max}} C_{\Delta Int,blend}\, dU \tag{6}$$

and calculating the inverse

$$U_{OCV,blend}(Q) = f^{-1}(U_{OCV,blend}(Q)). \tag{7}$$

Here U_{max} denotes the maximum potential and U_{min} the minimum potential of the blend cathode. The computation of $U_{OCV,blend}$ applying Equations (5)–(7) is very fast, which allows for online fitting, and the parameters β_i can be obtained from the fit.

Fig. 8 illustrates the complete procedure for the computation of an OCV curve of a blend cathode. It shows two hypothetical active materials, whose OCV curves exhibit a plateau at two different potentials. First of all, (i) the OCV curve for each single active material has to be measured or known, yielding $U_{OCV,1}$ and $U_{OCV,2}$. Second, (ii) the differential intercalation capacity is computed, yielding $C_{\Delta Int,1}$ and $C_{\Delta Int,2}$. Third, (iii) with the help of Equation (5) the individual differential intercalation capacities are scaled with

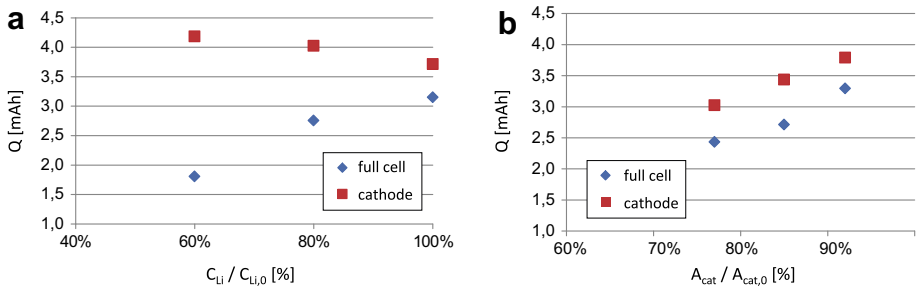

Fig. 5. a) Full cell and cathode capacity plotted versus the active lithium-ion content b) full cell and cathode capacity plotted versus the variation of the cathode active mass.

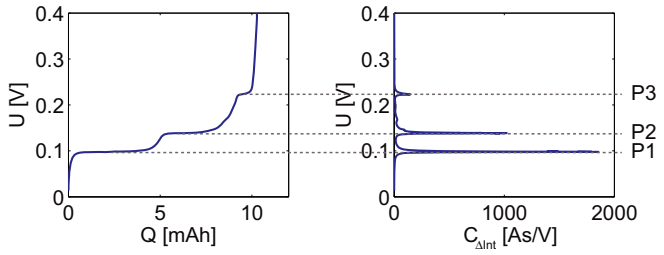

Fig. 6. OCV curve of a graphite electrode and resulting differential intercalation capacity plot. Normally $C_{\Delta Int}$ is plotted over the potential.

the factors β_i and added. Last, (iv) an integration of the previously obtained overall differential capacity $C_{\Delta Int,blend}$ applying Equation (6) results in the OCV curve $U_{OCV,blend}$.

3.2. Experimental

$LiNi_{0.8}Co_{0.15}Al_{0.05}O_2$ (NCA, Toda) and a stabilized $LiMn_2O_4$ spinel (LMO, Süd-Chemie) were used as active materials for the positive blend electrodes (compare Fig. 9a and b). The positive blend electrodes were prepared by mixing NCA and LMO in a 1:1 and 1:2 ratio (by wt.), as depicted in Fig. 9c. The composite positive electrodes consisted of the blended powder, conductive additives and polyvinylidene fluoride binder (PVdF, Solvay Solexis) in the weight ratio 92:4:4. Carbon black (Super P, Timcal) was chosen as conductive agent. *N*-methylpyrrolidone (NMP, Sigma Aldrich) was used as solvent. The resulting slurry was coated onto aluminum foil (22 μm thickness) using the doctor-blade technique and then dried at 80 °C to evaporate NMP. After that the film was dried overnight at 120 °C under vacuum to evaporate solvent and water residues in the composite electrode.

Experimental cells with a diameter of 18 mm were built using ECC-Ref cell housings (el-cell, Germany), which were equipped with a lithium reference electrode. As separator three Freudenberg FS2190 were used and 250 μl of LP50 (Merck, Germany) was used as electrolyte. The liquid electrolyte was composed of a 1 mol l^{-1} $LiPF_6$-solution in a 1:1 mixing ratio with ethylene carbonate:ethylmethyl carbonate (EC:EMC).

The cells were electrochemically characterized by charging and discharging at a current of C/40 using a Solartron 1470 Cell Test System (Solartron Analytical, GB) and a four wire set up. During the measurement the temperature was held constant at 25 °C by a WK3 climate chamber (Weiss, Germany).

3.3. Results

3.3.1. Measurements

Fig. 10a shows the reference OCV curves of the pure LMO and NCA cathodes, obtained by C/40 charge. The experimental cell made with LMO shows a higher potential during charging and a lower capacity. While the potential of the LMO cell varies between 3.9 V and 4.2 V, the potential of the NCA cell ranges from 3.6 V up to 4.2 V. It is therefore of common knowledge, that the intercalation of lithium into LMO is restricted to a more narrow voltage range when compared to NCA. This characteristic becomes even more obvious by comparing their differential intercalation capacity, where displayed in Fig. 10b. The potential plateaus are now visible as peaks, giving the characteristic intercalation potentials of NCA as $P_{1,NCA} = 3.57$ V, $P_{2,NCA} = 3.74$ V and $P_{3,NCA} = 3.98$ V (compare reference [20]) and for LMO at $P_{1,LMO} = 4.03$ V and $P_{2,LMO} = 4.15$ V [21].

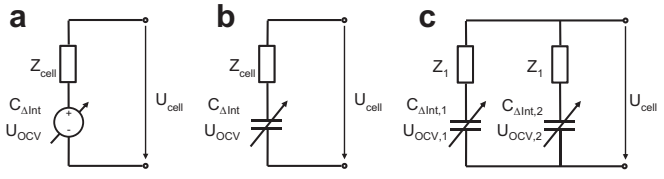

Fig. 7. Equivalent circuits for lithium-ion cells: a) ordinary equivalent circuit with a potential source as representation of the OCV, b) equivalent circuit applying a controlled capacity for representation of the OCV, c) equivalent circuit for the simulation of blends consisting of two different active materials.

Fig. 11a represents the OCV curves measured for an experimental cell with blend ratios for NCA/LMO of 1:1 (blue in the web version) and 1:2 (green in the web version). Comparing the blend ratio 1:1 with the peak potentials of the LMO and NCA cathodes in Fig. 11b, one can resemble the peaks $P_{1,NCA}$ and $P_{2,NCA}$ of NCA as well as $P_{2,LMO}$ of LMO. The peak at 4.02 V is a superposition of $P_{3,NCA}$ and $P_{1,LMO}$. As expected, the differential capacity of a blend results in a superposition of the differential intercalation capacities of its individual cathode materials. The minor accordance of the peak at the lowest potential is discussed later.

Comparing now the blend ratio 1:2 with the peak potentials of the LMO and NCA cathodes in Fig. 10b, the peak potentials are sustained, but the area beneath the peaks differs clearly from the blend ratio 1:1. Now we proceed with using our *OCV model blend cathode* and determine the scaling factors β_i of the actual two blend ratios. The procedure and the results are discussed in the following section.

3.3.2. Simulation and analysis

The *OCV model blend cathode* uses as data basis the obtained OCV curves of the individual LMO and NCA cathodes shown in Fig. 10. As already stated, and in contrast to the prediction of OCV curves of blend electrodes, the scaling factors are not set a priori. They have to be determined by a fit procedure using the measured OCV of the blend electrode. As quality criterion the sum of squared error of the simulated and measured differential intercalation capacity is chosen. The fit result is depicted in Fig. 12 as dotted line. Whereas deviations are hardly visible in the OCV curve (compare Fig. 12b), slight deviations are unveiled by the differential intercalation capacity plot (compare Fig. 12a). As mentioned before, the peak with the lowest potential is not described accurately by the model and therefore the potential range of the fit was restricted to potentials above this peak. Reasons for this deviation are discussed in the next section.

The scaling parameters β_i yielded by the fit, can now be used to determine the mass ratio of the individual blend components. The computed active masses are depicted together with the values from the electrode preparation in Fig. 13.

3.4. Discussion

Fig. 11b gives evidence, that deviations of the simulated OCV curves, which are fitted by the *OCV model cathode blend*, are below 25 mV for both blend cathodes. The peak potentials of the calculated differential intercalation capacities (compare Fig. 12a), are in good accordance with the measurement and reflect the characteristic behavior of the constituents NCA and LMO. The error for the estimated mass ratios is lower as 9% for the blend ratio of 1:1 and lower as 6% for the blend ratio of 1:2. It is obvious, that an error of 9% of the estimated total active mass, which correlates with the total capacity, strongly affects the estimation of the components mass ratio. This underestimation is partly explainable by the insufficient coulombic efficiency during slow C/40 cycles. Thereby, side reactions influence the measured capacity, which are not

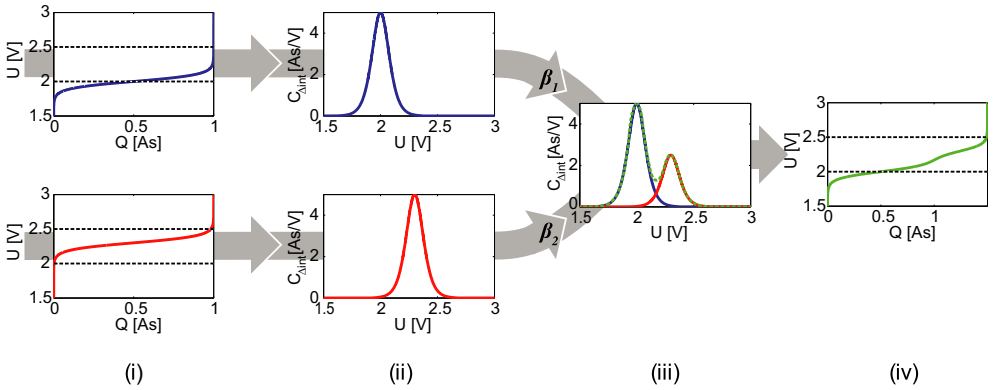

Fig. 8. Procedure for the computation of the OCV of a blend electrode: (i) measurement of the OCV of the single blend components, (ii) computation of the differential intercalation capacity $C_{\Delta Int,i}$, (iii) scaling of $C_{\Delta Int,i}$ for each component by multiplication with the scaling factors β_1, β_2 and subsequent addition, (iv) computation of the OCV curve.

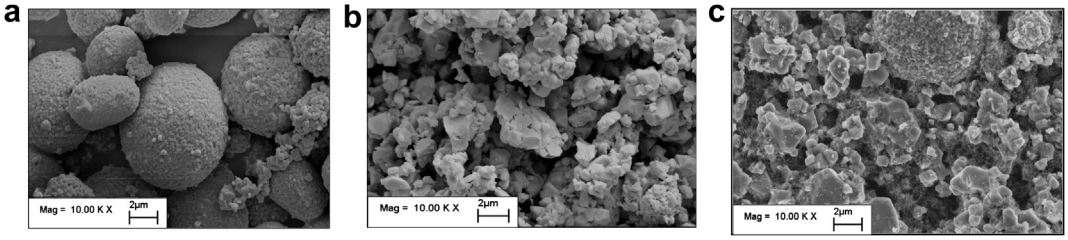

Fig. 9. SEM images of the a) NCA powder, b) LMO powder and c) the blend electrode.

covered by the *OCV model cathode blend*. Increasing the coulombic efficiency is therefore key issue for increasing the accuracy of the diagnosis of blend cathodes.

As mentioned earlier, the fitted potential range is limited to potentials above 3.7 V, and the peak with the lowest potential is omitted. This peak originates from the NCA and its potential of 3.57 V slightly differs from the potential of 3.59 V determined in both blends. We assume this deviation to be caused by the different dynamic behavior of the blend cathode and not by an altered intercalation potential. At low potentials the impedance increases

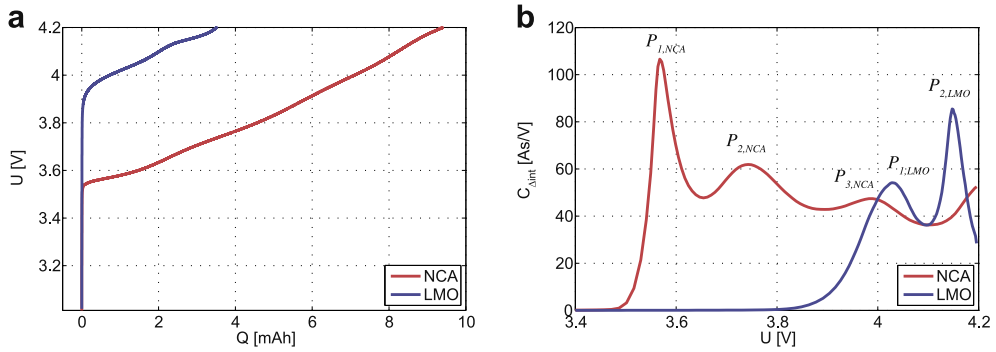

Fig. 10. a) OCV curves of NCA and LMO electrodes, obtained by C/40 charging b) differential intercalation capacity of NCA and LMO electrodes, characteristic peak potentials are highlighted for NCA $P_{1,NCA} = 3.57$ V, $P_{2,NCA} = 3.74$ V, $P_{3,NCA} = 3.98$ V and for LMO $P_{1,LMO} = 4.03$ V, $P_{2,LMO} = 4.15$ V.

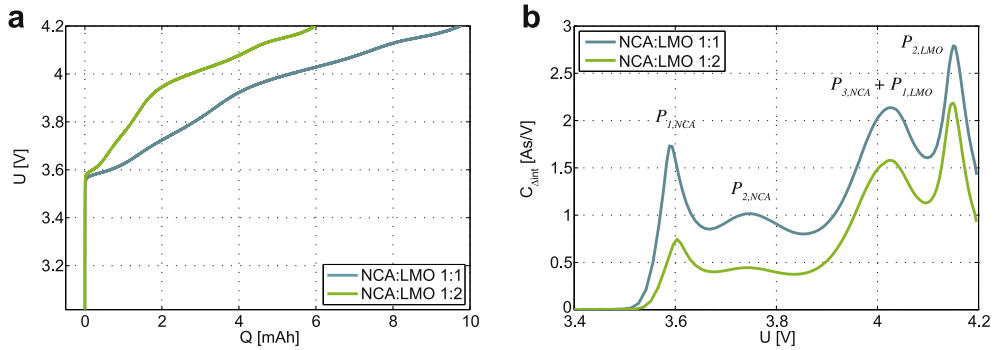

Fig. 11. a) OCV curves obtained by C/40 charging of NCA/LMO blend cathodes with a ratio of 1:1 and 1:2 b) differential intercalation capacity of the blend electrodes.

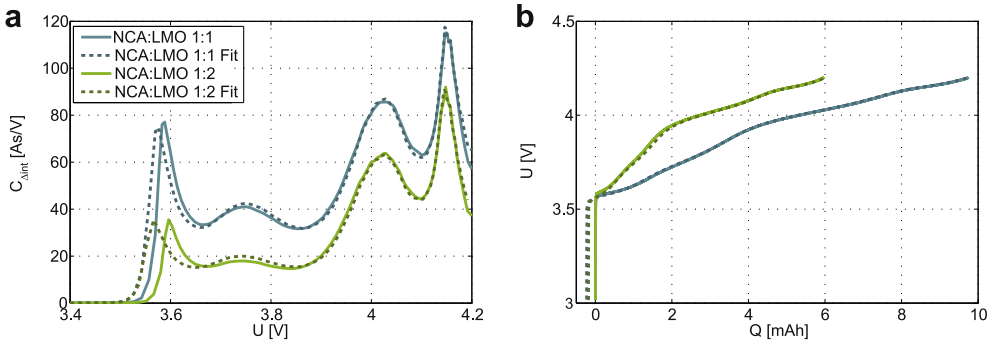

Fig. 12. Measured (straight line) and fitted (dotted line) differential intercalation capacity of the blend cathodes with a ratio of 1:1 and 1:2.

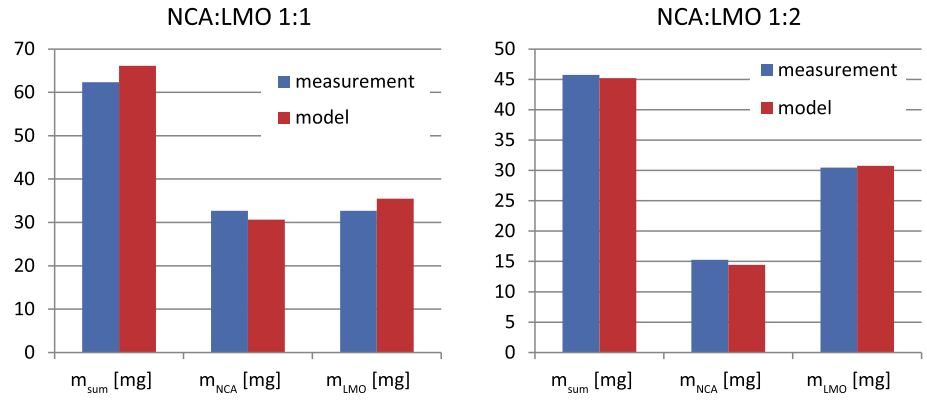

Fig. 13. Comparison of the overall active material mass and the masses of the individual blend components obtained by the model fit with measured values from electrode preparation.

rapidly and thus the dynamic behavior becomes dominant. Therefore, our before made assumption, that a slow charge or discharge reflects the OCV closely, does not hold true anymore. Since the blends, when compared to the pure NCA, feature microstructures differing in electronic and ionic conducting pathways, the dynamic behavior also varies.

The particle model proposed by Albertus et al. [22] implements the dynamic behavior of a NCA/LMO blend electrode based on physically motivated differential equations while the OCV of NCA and LMO are represented as Look up table. If all material parameters are known, the model is suitable to predict the dynamic behavior. However, the computation effort is rather high, impeding the online analysis of the slow discharge of blends. Therefore the combination of the introduced *OCV model cathode blend* with the impedance model introduced in Ref. [23] will be part of future work, as it promises low computation effort resulting in good real-time capability.

4. Conclusion

A model approach is presented, which allows for a quantitative analysis as well as prediction of the open circuit potential of lithium-ion cells (*OCV model full-cell*). Furthermore, this model determines half-cell potentials of already stressed lithium-ion cells, using a data set accomplished just once from half-cell potentials of a new reference cell. To the cost of one disassembled cell, further cells of the same chemistry can be analyzed then without destruction. With the help of the *OCV model full-cell*, two relevant degradation processes, namely (i) loss of active mass and (ii) loss of active lithium, were experimentally verified on a NCA/LCO blend cell. Therefore this model has a potential for investigating aging in field tests.

Furthermore, an extended model (*OCV model blend cathode*) was proven to predict (i) the open circuit potential of a blend cathode with various blend ratios as well as (ii) the analysis of unknown blend ratios. This ability was validated successfully for cathodes made of NCA/LMO blends. Therefore this extended model is also suitable for investigating the degradation of blend cathodes. The simple structure and the low computation effort of both models allow for online diagnosis.

Acknowledgments

Part of this work was supported by Deutsche Forschungsgemeinschaft (DFG, Functional materials and material analysis for lithium high power batteries), by the Federal Ministry of Education and Research within the Framework Concept KoLiWIn (fund number 03SF0343H) and Elektrochemie für Elektromobilität – Verbund Süd (fund number 03KP801), managed by the Project Management Agency Forschungszentrum Jülich (PTJ). All responsibility for this publication rests with authors.

References

[1] A.J. Bard, L.R. Faulkner, Electrochemical Methods Fundamentals and Applications, John Wiley & Sons, Inc., New York, 2001.
[2] M.S. Wu, P.C.J. Chiang, J.C. Lin, J. Electrochem. Soc. 152 (2005) A47–A52.
[3] Y. Zhang, C.Y. Wang, J. Electrochem. Soc. 156 (2009) A527–A535.
[4] J. Zhou, P.H.L. Notten, J. Electrochem. Soc. 151 (2004) A2173–A2179.
[5] D.P. Abraham, J. Liu, C.H. Chen, Y.E. Hyung, M. Stoll, N. Elsen, S. MacLaren, R. Twesten, R. Haasch, E. Sammann, I. Petrov, K. Amine, G. Henriksen, J. Power Sources 119–121 (2003) 511–516.

[6] A.N. Jansen, D.W. Dees, D.P. Abraham, K. Amine, G.L. Henriksen, J. Power Sources 174 (2007) 373–379.
[7] G. Nagasubramanian, Impedance studies on cathodes in Li-ion cells, in: Energy Conversion Engineering Conference and Exhibit, 2000. (IECEC) 35th Intersociety, 2000, pp. 968–975.
[8] K. Honkura, H. Honbo, Y. Koishikawa, T. Horiba, ECS Trans. 13 (2008) 61–73.
[9] M. Dubarry, C. Truchot, B.Y. Liaw, J. Power Sources 219 (2012) 204–216.
[10] J. Dahn, G.M. Ehrlich, Lithium-ion batteries, in: T.B. Reddy (Ed.), Linden's Handbook of Batteries, Mcgraw-Hill Professional, New York, 2010.
[11] H.Y. Tran, C. Täubert, M. Fleischhammer, P. Axmann, L. Küppers, M. Wohlfahrt-Mehrens, J. Electrochem. Soc. 158 (2011) A556–A561.
[12] M. Dubarry, V. Svoboda, R. Hwu, B.Y. Liaw, Electrochem. Solid State Lett. 9 (2006) A454–A457.
[13] I. Bloom, A.N. Jansen, D.P. Abraham, J. Knuth, S.A. Jones, V.S. Battaglia, G.L. Henriksen, J. Power Sources 139 (2005) 295–303.
[14] K. Honkura, K. Takahashi, T. Horiba, J. Power Sources 196 (2011) 10141–10147.
[15] M. Dubarry, B.Y. Liaw, J. Power Sources 194 (2009) 541–549.
[16] M. Safari, C. Delacourt, J. Electrochem. Soc. 158 (2011) A1123–A1135.
[17] P. Liu, J. Wang, J. Hicks-Garner, E. Sherman, S. Soukiazian, M. Verbrugge, H. Tataria, J. Musser, P. Finamore, J. Electrochem. Soc. 157 (2010) A499–A507.
[18] J. Vetter, P. Novak, M.R. Wagner, C. Veit, K.C. Möller, J.O. Besenhard, M. Winter, M. Wohlfahrt-Mehrens, C. Vogler, A. Hammouche, J. Power Sources 147 (2005) 269–281.
[19] M.D. Levi, D. Aurbach, Electrochim. Acta 45 (1999) 167–185.
[20] D.P. Abraham, S. Kawauchi, D.W. Dees, Electrochim. Acta 53 (2008) 2121–2129.
[21] M. Winter, J.O. Besenhard, M.E. Spahr, P. Novak, Adv. Mater. 10 (1998) 725–763.
[22] P. Albertus, J. Christensen, J. Newman, J. Electrochem. Soc. 156 (2009) A606–A618.
[23] J.P. Schmidt, P. Berg, M. Schönleber, A. Weber, E. Ivers-Tiffée, J. Power Sources 221 (2013) 70–77.